Highly sensitive biochemical sensor utilizing Bragg grating in submicron Si/SiO_2 waveguides

Saurabh Mani Tripathi*[a], Arun Kumar[a], Jean-Pierre Meunier[b] and Emmanuel Marin[b]
[a] Physics Department, Indian Institute of Technology, Hauz Khas, New Delhi, INDIA 110016;
[b] Laboratoire Hubert Curien, Université de Lyon, F-42023, CNRS, UMR n°5516, Université de Saint-Etienne, F-42023, Saint-Etienne, FRANCE 42000.

ABSTRACT

We present a novel highly sensitive biochemical sensor based on a Bragg grating written in the cladding region of a submicron planar Si/SiO_2 waveguide. Owing to the high refractive index contrast at the Si/SiO_2 boundary the TM modal power is relatively high in low refractive index sensing region, leading to higher sensitivity in this configuration [1]. Waveguide parameters have been optimized to obtain maximum modal power in the sensing region (P_{Se}) and an optimum core width corresponding to maximum sensitivity is found to exist while operating in TM mode configuration, as has been shown in Fig. 1. It has been found that operating in TM mode configuration at optimum core width the structure exhibits extremely high sensitivity, ~ 5×10^{-6} RIU – 1.35×10^{-6} RIU for the ambient refractive indices between 1.33 – 1.63. Such high sensitivities are typically attainable for Surface Plasmon Polariton (SPP) based biosensors and is much higher than any non SPP based sensors. Being free from any metallic layer or bulky prism the structure is easy to realize. Owing to its simple structure and small dimensions the proposed sensor can be integrated with planar lightwave circuits and could be used in handy lab-on-a-chip devices. The device may find application in highly sensitive biological/chemical sensing areas in civil and defense sectors where analyzing the samples at the point of need is required rather than sending it to some centralized laboratory.

Keywords: Bragg grating, refractive index sensor, integrated optic waveguide, submicron waveguide, semiconductor on insulator, lab-on-a-chip device.

1. INTRODUCTION

In the recent past there has been a growing interest in miniaturizing optical components so that the whole of the optical assembly could be fabricated on a single chip with submicron size components [1-4]. The ease of fabricating simple and well defined waveguide structures using silica make Si/SiO_2 waveguides the most promising candidate to fabricate these so called lab-on-a-chip (LOC) devices [5]. Owing to their submicron size these devices require much smaller amount of the sample and the quantity of chemical/biological waste can thus be much reduced. Typically Surface Plasmon Polariton (SPP) and Bragg grating based sensors are used for biochemical sensing applications as they have some unique advantages over other schemes. One of the main advantages is that the measured information is wavelength encoded. As a result, these sensors are free from referencing and are immune to fluctuations in the input light intensity and connector losses. Amongst the two, the SPP based sensors exhibit higher sensitivity [6-10] due to the increased modal field at the metal/dielectric boundary [6]. They, however, either use a bulky prism, as in Kretschmann configuration, [6] or face difficulty in exiting a pure SPP as in the case of a SPP based fiber gratings based sensor [7]. In this paper we propose and analyze a new biochemical sensor consisting of a high index Silicon core and a Bragg grating written in the photo sensitive cladding region. The structure can be realized using a Si substrate over which are grown a lower cladding of SiO_2, a Si core, an upper cladding of GeO_2 doped SiO_2 followed by the sensing region. Owing to the high refractive index difference between the Si and SiO_2 materials the TM mode has a large field in the cladding region, similar to that of a slot waveguide [2], and hence a large field in the sensing region as well. As the gratings are difficult to be inscribed in photo insensitive Si core region [11] we propose them to be inscribed in the photo sensitive upper cladding made of GeO_2 doped SiO_2. The results presented here are general and can be extended to rectangular or cylindrical geometries.

*tripathi.iit@gmail.com; phone +91 11 2659-6579; fax +91 11 2658-2037;

Fiber Optic Sensors and Applications VI, edited by Eric Udd, Henry H. Du, Anbo Wang, Proc. of SPIE Vol. 7316, 73160J
© 2009 SPIE · CCC code: 0277-786X/09/$18 · doi: 10.1117/12.818464

2. THE STRUCTURE AND ITS ANALYSIS

The schematic diagram of the proposed planar sensor structure along with the coordinate system to analyze it is shown in Fig.1. It is infinitely extended along '*x*' and '*y*' directions, with '*x*' being the direction of refractive index variation, and the '*z*' direction has been taken as the direction of propagation. The core and cladding widths are taken as *a* and *b*, respectively, and n_{lcl}, n_c, n_{ucl} and n_s are the uniform refractive indices of the lower cladding, core, upper cladding and sensing regions, respectively. The lower cladding and the sensing regions are of the order of a few microns so that the evanescent field does not see the presence of any region beyond them. We have used the vector modal analysis [12, 13] to study the mode propagation characteristics of the analyze structure and the standard Coupled mode theory (CMT) [14] to study the power coupling between the forward and backward propagating guided modes. The standard wave equations in TE and TM mode configuration are given as [12,13],

$$\frac{d^2E_y}{dx^2}+\left[k_0^2n^2(x)-\beta^2\right]E_y=0 \tag{1}$$

and

$$\frac{d^2H_y}{dx^2}-\left[\frac{1}{n^2(x)}\frac{dn^2}{dx}\right]\frac{dH_y}{dx}+\left[k_0^2n^2(x)-\beta^2\right]H_y=0 \tag{2}$$

respectively. For the non perturbed structure the propagation constant (β) and the field distribution are obtained by satisfying appropriate boundary conditions, which in TE mode configuration are continuity of E_y and $\frac{dE_y}{dx}$, and in TM mode configuration are continuity of H_y and $\frac{1}{n^2}\frac{dH_y}{dx}$, at various dielectric discontinuities. The fields are then normalized to carry unit power. Once the modal propagation constant and field distributions have been obtained the power coupling could be obtained as follows. The refractive index perturbation describing the grating can be written as [14]

$$\delta n_{ucl}=n_{ucl}\sigma\left(1+\upsilon\cos\left(\frac{2\pi}{\Lambda}z\right)\right) \tag{3}$$

where 'σ' is the grating strength (GS) such that $n_{ucl}\sigma$, is equal to the maximum index change in the grating region, 'υ' is the visibility of the_fringes, and Λ is the grating period. Using the CMT it is well known that the maximum coupling between forward and backward propagating core modes occurs at the resonance wavelength λ_R, satisfying the phase matching condition,

$$\kappa_{co-co}+\beta-\frac{\pi}{\Lambda}=0 \quad\Rightarrow\quad \lambda_R=2\Lambda\left(n_{eff}+\frac{\kappa_{co-co}}{k_0}\right) \tag{4}$$

where n_{eff} (= β/k_0) is the effective index of guided core mode, k_0 is the free space wave number and κ_{co-co} is the core mode to core mode coupling coefficient, given by,

$$\kappa_{co-co}=\frac{k_0n_{ucl}^2\times\sigma}{2Z_0}\int_a^{a+b}\left|E_i\right|^2dx \tag{5}$$

And '*i*' is '*x*' or '*y*' for TM or TE modes, respectively, and Z_0 (= 120π Ω) is the characteristic impedance of the free space. Further, according to Eq. 4, by selecting the grating parameters appropriately we can tune the resonance at any desired wavelength. The grating assisted power coupling to backward propagating guided mode and hence the reflectivity is obtained by the relation [14],

$$R=\frac{\left[\left|\kappa_{co-co}\right|\times\sinh\left(\alpha\times L\right)\right]^2}{\left[\left|\kappa_{co-co}\right|\times\cosh\left(\alpha\times L\right)\right]^2-\delta^2} \tag{6}$$

where, $\delta = \left(\kappa_{co-co} + \beta - \frac{\pi}{\Lambda} \right)$ is the detuning parameter and $\alpha = \sqrt{\left|\kappa_{co-co}\right|^2 - \delta^2}$. At the resonance wavelength, $\delta = 0$ and hence the reflectivity can be written as $R(\lambda_R) = \tanh^2(\left|\kappa_{co-co}\right| L)$, using this relation the required grating length 'L' to achieve a desired reflectivity at the resonance wavelength can be determined. In our calculations the upper cladding region is considered to be made of 4.1 mol% GeO_2 doped SiO_2. The refractive index of the core region is taken as 3.48, and that of the cladding regions are obtained by using the well known Sellmeier relations [12]

$$n^2(\lambda) - 1 = \sum_{j=1}^{3} \frac{A_j \lambda^2}{\lambda^2 - B_j^2} \tag{7}$$

where, A_j and B_j are Sellmeier coefficients. Typical values of refractive indices of lower and upper cladding regions calculated at an operating wavelength 1.55 μm are 1.444 and 1.4503, respectively. The GS has been fixed at 5×10^{-4} and the reflectivity has been taken as 0.7 (i.e. 70% of the input power). Changing the ARI changes the propagation constant of the guided mode and hence the resonance wavelength λ_R. Thus, by measuring this shift in λ_R the changes in ARI could be measured by defining the sensitivity as the rate of change of resonance wavelength λ_R with respect to unit change in ARI, *i.e.* sensitivity = $\Delta\lambda_R/\Delta n_s$, in the units of nm/ RIU.

3. RESULTS AND DISCUSSION

In this section we first present effective index variation with respect to ARI, for both the TE_0 mode (Fig.2(a)) and TM_0 mode (Fig.2(b)), for the above mentioned waveguide having arbitrarily chosen parameters of a = 0.17 μm and b = 0.10 μm. The operating wavelength has been taken as 1.55 μm. From this figure two observations can be easily made,

1. The TM_0 mode has lower effective index as compared to that of TE_0 mode implying relatively weekly guiding of TM_0 mode.
2. Effective indices of both the TE_0 and TM_0 modes increase with increasing ARI with TM_0 mode effective index being more sensitive than that of TE_0 mode, with the former varying by nearly 4% as compared to nearly 0.3% change in TE_0 modes effective index over the ARI range considered in the figure.

Typically the TM mode is known to have lower effective index than the TE mode [12,13] and therefore relatively more sensitive to ARI changes. However the n_{eff} does not vary such rapidly in conventional waveguides. Having obtained the effective indices for both the modes it is now interesting to observe the normalized transverse electric field extension, namely the E_x and E_y components for TM_0 mode and TE_0 mode respectively, in various regions of the waveguide. As has been shown in Fig.3 for the TM_0 mode due to the n_i^2/n_j^2 discontinuity at every '*i-j*' boundary the field in the cladding and sensing regions is much larger as compared to that of the TE_0 mode, and indeed it is this increased field in the ARI region which makes the TM_0 mode more sensitivity to the changes in ARI region as compared to the TE_0 mode. This is further clear from Fig.4 where we have plotted the ARI sensitivity (=$\Delta\lambda_R/\Delta n_{se}$), in terms of the shift in the resonance wavelength per refractive index unit (RIU) change in ARI region, as a function of core width for both the TM_0 mode and the TE_0 modes. The required grating period and grating length for every core width have been calculated for the same operating wavelength of 1.55 μm and an ARI of 1.33. An interesting observation here is that there exists an optimal core width 0.13 μm at which the TM_0 mode based sensor is maximum sensitive, the corresponding grating period and grating lengths being 0.509 μm and 3.2 mm, respectively. This behavior can be attributed to the asymmetric geometry of the waveguide structure, and to understand it more clearly in Fig.5 we have presented the fractional modal power of TM_0 mode in various regions of the waveguide as a function of core width. As can be observed the power in the sensing region shows a maximum near a core width of 0.13 μm coinciding with the observed optimum core width. We would like to point out here that such an optimum core width (~0.028 μm) exists for TE_0 mode also; however the sensitivity is still inferior as compared to that of the TM_0 mode. Further, as is well understood, the modal field has a tendency to shift towards higher refractive indices [12,13] the sensor should be more sensitive for higher index samples. In order to see the effect of ARI on the optimum core width, in Fig.6, we have plotted the fractional modal power in the sensing as well as the substrate region as a function of core width for different overlay refractive indices. As can be observed, increasing ARI results in an increased modal power in the sensing region and causes the optimum core width to shift towards lower values and finally disappear at higher ARIs. On the other hand at higher overlay refractive indices the modal power in the substrate region starts showing maximum at a certain core width in an exactly opposite manner as has been shown in the sensing region, though the behavior of optimum core width shifting towards higher value with lower field in the concerned region is similar in both the cases.

Now in order to optimize the structure for maximum sensitivity it is imperative to study the cumulative effect of the upper cladding width, the core width and the ARI on the sensor performance. To study this, in Fig.7 we have plotted the variation of the fractional modal power in the sensing region 'P_S' with both core and upper cladding widths. As is evident there is no such optimum upper cladding width, however the optimum core width ('a_{opt}') exists for every 'b', shifting towards higher values with reducing 'b'. It can be observed that reducing the upper cladding thickness b improves the sensitivity because of the increased power in the sensing region. However, the required grating length to attain the same reflected power (70%) has to be increased considerably because of the reduced modal overlap within the grating region. For example, we found that at an ARI of 1.33 and for optimized core width of 0.13 μm, the required grating length is 6.9 mm for b = 0.05 μm as compared to that of 3.2 mm at b = 0.1 μm. The corresponding sensitivities being 4.17×10^{-6} RIU and 5×10^{-6} RIU. Changing the ARI, however, greatly affects the sensor performance due to the guided modes tendency to be shifted towards higher refractive index regions. As can be observed from Fig.8 where we have plotted the variation of the resonance wavelength λ_R and the minimum detectable change in the ARI assuming that the detector has a resolution of 1 pm, for the sensor parameters of a = 0.13 μm, b = 0.1 μm, Λ = 0.509 μm and L = 3.2 mm. As is clear the sensitivity increases for higher refractive index samples due to the increased modal field in high index ARI region. Changes as small as 5×10^{-6} RIU – 1.35×10^{-6} RIU could be detected for biochemical sample between 1.33 – 1.63 which is nearly twice the order of magnitude better than the conventional Bragg grating based sensor using integrated optic (1×10^{-4} RIU) or fiber optic (1.4×10^{-5} RIU) waveguides [8,9] and is of the order of SPP based sensors [10]. Thus, not only such a scheme has a better sensitivity, it can well be used over a large variety of bio/chemical samples.

4. CONCLUSION

In summary, we have presented a novel highly sensitive submicron Si/SiO_2 waveguide refractive index sensor with the Bragg grating inscribed in its cladding region. An optimum core width corresponding to maximum sensitivity is found to exist for both the TE_0 and TM_0 mode configurations. The simulated sensitivity is comparable to that of SPP based sensors. Being free from any metallic layer or moving part the presented sensor is preferable over the SPP based schemes. Due to its small over all dimensions and planar structure it can be easily integrated with handy lab-on-a-chip device for biological/chemical sensing applications.

5. FIGURES

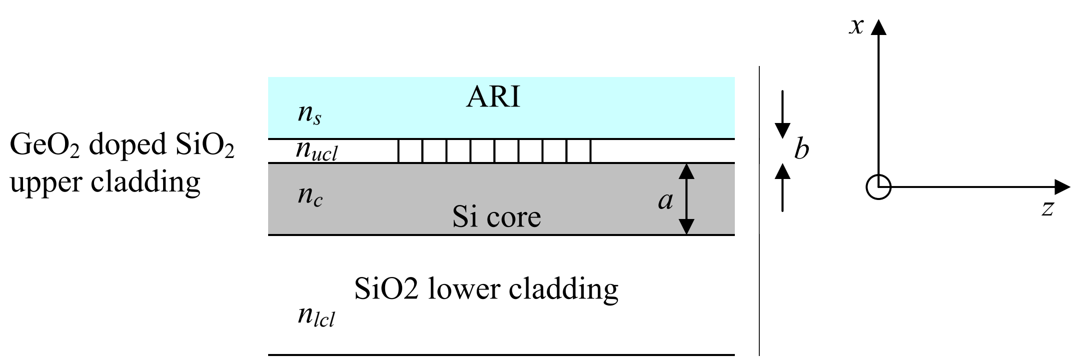

Fig. 1. Schematic diagram of the sensor structure and its coordinate system.

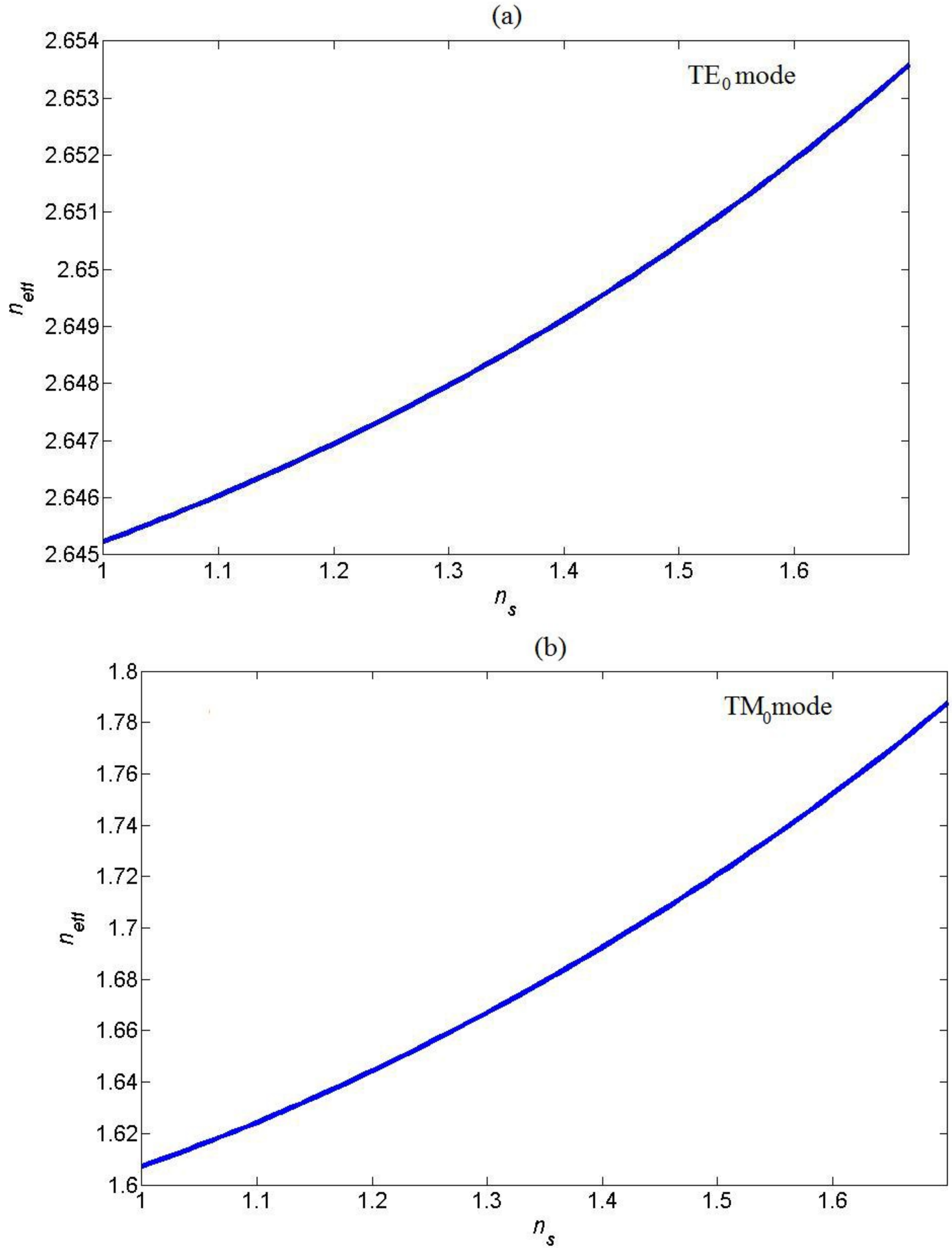

Fig. 2. Effective index variation with respect to ARI (n_s) for (a) TE_0 mode and (b) TM_0 mode, for a = 17 μm and b = 0.1 μm.

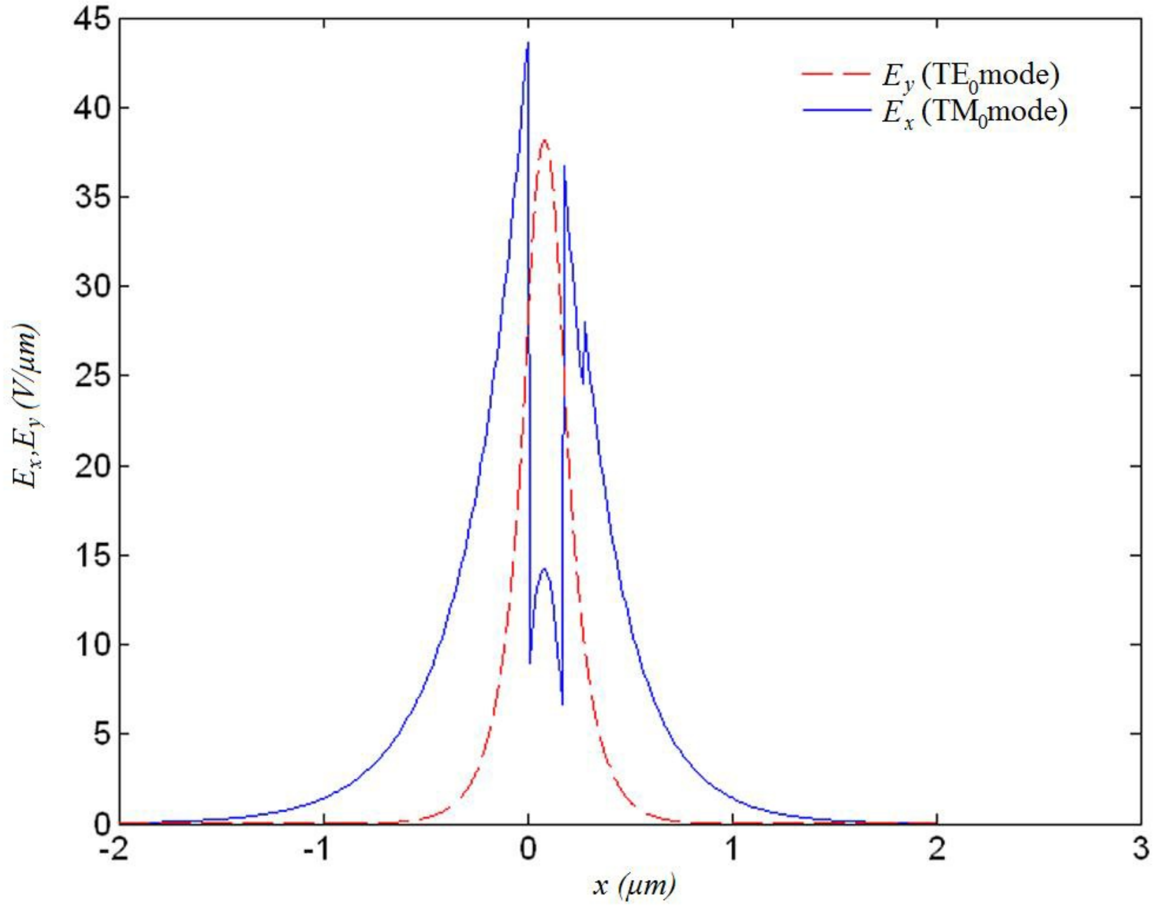

Fig. 3. Normalized field extension for TE_0 mode and TM_0 mode for a = 17 μm and b = 0.1 μm.

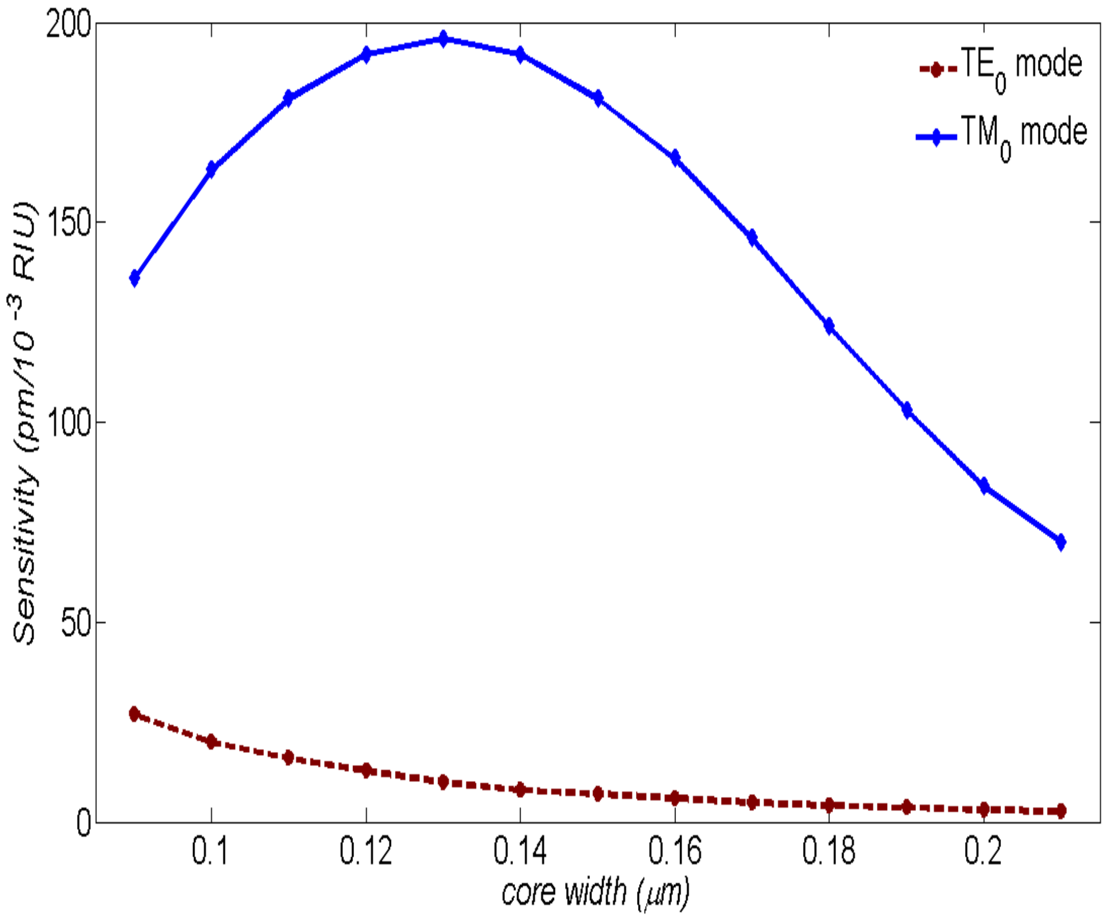

Fig. 4. Sensitivity variation with respect to core width. An optimum core width at 0.13 µm exists for TM_0 mode.

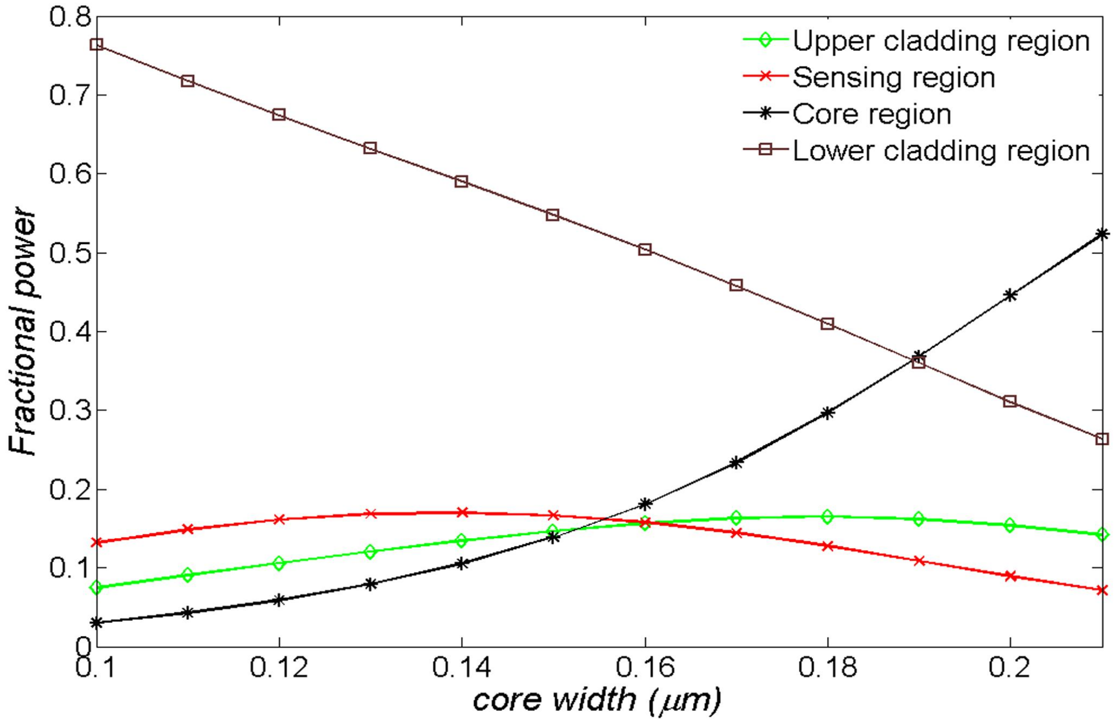

Fig. 5. Fractional modal power in different regions of the waveguide as a function of core width.

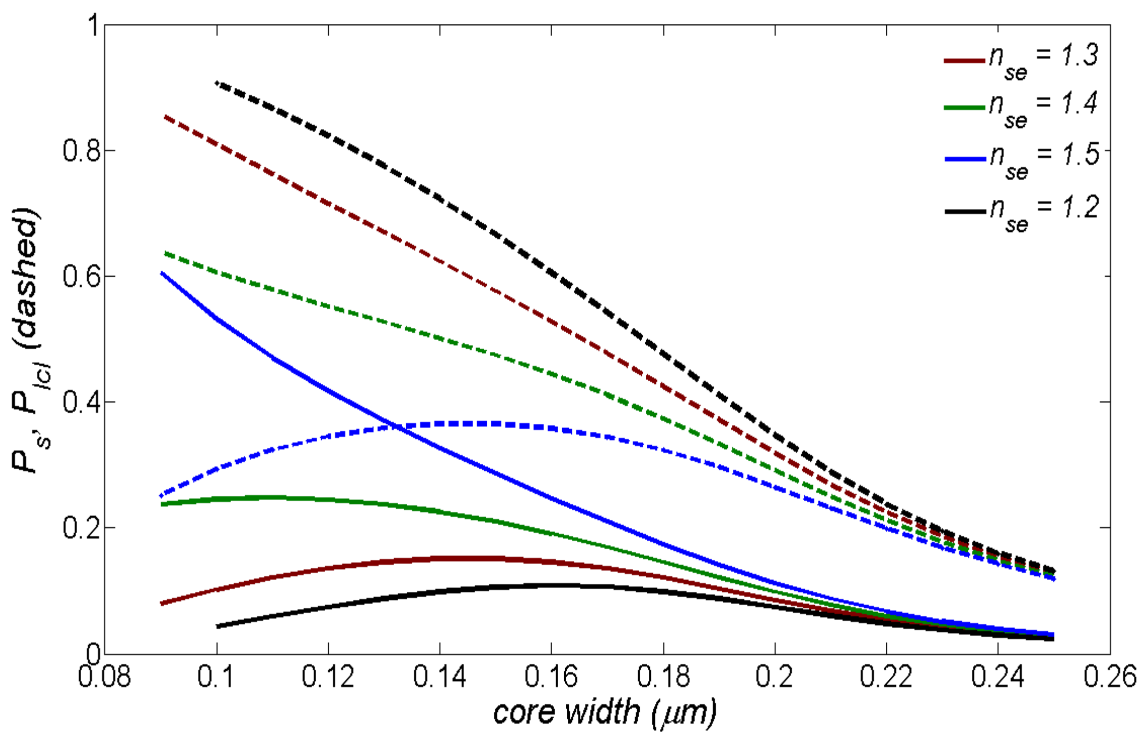

Fig. 6. Fractional modal power of TM_0 mode in sensing and lower cladding regions as a function of core width.

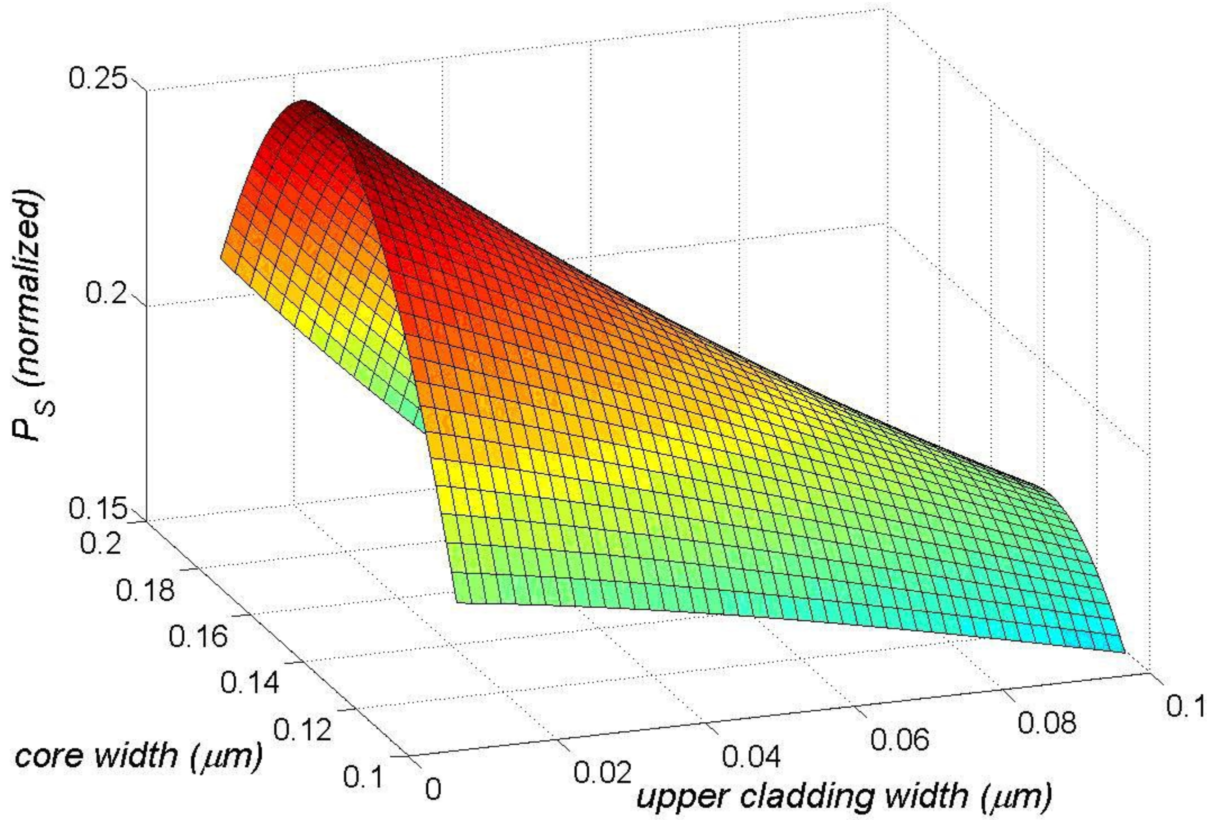

Fig. 7. Optimization of waveguide parameters to maximize fractional modal power in sensing region.

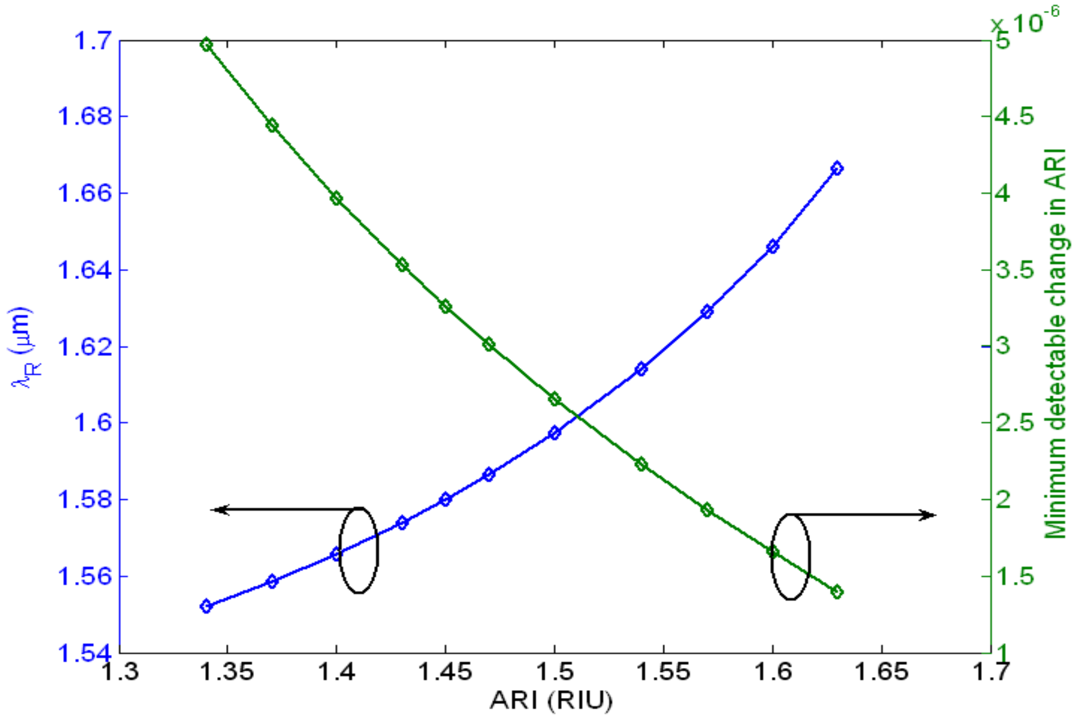

Fig. 8. Resonance wavelength (λ_R) and ARI sensitivity variation with ARI for a = 0.13 μm and b = 0.1 μm.

REFERENCES

[1] Kawachi, M., "Silica waveguides on silicon and their application to integrated-optic components", Opt. Quantum Electron., 22, 391-416, (1990).

[2] Almeida, V. R., Xu, Q., Barrios, C. A., and Lipson, M., "Guiding and confining light in void nanostructure", Opt. Lett., 29, 1209-1211, (2004).

[3] Xu, Q., Almeida, V. R., Panepucci, R. R., and Lipson, M., "Experimental demonstration of guiding and confining light in nanometer-size low-refractive-index material", Opt. Lett., 29, 1626-1628, (2004).

[4] Lee, K. K., Lim, D. R., and Kimerling, L. C., "Fabrication of ultralow-loss Si/SiO_2 waveguides by roughness reduction", Opt. Lett., 26, 1888-1890, (2001).

[5] *Nature:Insight: Lab on a chip,* 442, 367-418, (2006).

[6] Reather H., [Surface Plasmons on Smooth and Rough Surfaces and on Gratings], Springer, New York, 1986.

[7] Shevchenko, Y. Y. and Albert, J., "Plasmon resonances in gold-coated tilted fiber Bragg gratings", Opt. Lett, 32, 211-213, (2007).

[8] Liang, W., Huang, Y., Xu, Y., Lee, R. K., and Yariv, A., "Highly sensitive fiber Bragg grating refractive index sensors", Appl. Phys. Lett., 86, 151122(1)-151122(3), (2005).

[9] Emmerson, G. D., Gawith, C. B. E., Sparrow, I. J. G., Williams, R. B., and Smith, P. G. R., "Physical observation of single step UV-written integrated planar Bragg structures and their application as a refractive-index sensor", Appl. Opt., 44, 5042-5045, (2005).

[10] Tripathi, S. M., Kumar, A., Marin, E., and Meunier, J-P, "Side-Polished Optical Fiber Grating Based Refractive Index Sensors Utilizing the Pure Surface Plasmon Polariton", IEEE J. Lightwave Technol., 26, 1980-1985, (2008).
[11] Albert, J., Fokine, M. and Margulis, W., "Grating formation in pure silica-core fibers", Opt. Lett, 27, 809-811, (2002).
[12] Adams, M. J., [An Introduction to Optical Waveguides], Chapter 2 and 7, Wiley, New York, (1981).
[13] Okamoto, K., [Fundamentals of Optical Waveguides], chapter 2, Academic Press, San Diego, (2000).
[14] Kashyap, R., [Fiber Bragg Gratings], Chapter 4, Academic Press, San Diego, (1999).